SANDIA REPORT
SAND2010-5687
Unlimited Release
Printed September 2010

Optoelectronic and Excitonic Properties of Oligoacenes and One-Dimensional Nanostructures

Bryan M. Wong and Timothy H. Hsieh

Prepared by
Sandia National Laboratories
Albuquerque, New Mexico 87185 and Livermore, California 94550

Sandia National Laboratories is a multi-program laboratory managed and operated by Sandia Corporation, a wholly owned subsidiary of Lockheed Martin Corporation, for the U.S. Department of Energy's National Nuclear Security Administration under contract DE-AC04-94AL85000.
.

Issued by Sandia National Laboratories, operated for the United States Department of Energy by Sandia Corporation.

Available to DOE and DOE contractors from
U.S. Department of Energy
Office of Scientific and Technical Information
P.O. Box 62
Oak Ridge, TN 37831

Telephone: (865) 576-8401
Facsimile: (865) 576-5728
E-Mail: reports@adonis.osti.gov
Online ordering: http://www.osti.gov/bridge

Available to the public from
U.S. Department of Commerce
National Technical Information Service
5285 Port Royal Rd.
Springfield, VA 22161

Telephone: (800) 553-6847
Facsimile: (703) 605-6900
E-Mail: orders@ntis.fedworld.gov
Online order: http://www.ntis.gov/help/ordermethods.asp?loc=7-4-0#online

SAND2010-5687
Unlimited Release
Printed September 2010

Optoelectronic and Excitonic Properties of Oligoacenes and One-Dimensional Nanostructures

Bryan M. Wong and Timothy H. Hsieh

Materials Chemistry Department
Sandia National Laboratories
P.O. Box 969, MS 9403
Livermore, CA. 94551-0969

Abstract

The optoelectronic and excitonic properties in a series of linear acenes are investigated using range-separated methods within time-dependent density functional theory (TDDFT). In these highly-conjugated systems, we find that the range-separated formalism provides a substantially improved description of excitation energies compared to conventional hybrid functionals, which surprisingly fail for the various low-lying valence transitions. Moreover, we find that even if the percentage of Hartree-Fock exchange in conventional hybrids is re-optimized to match wavefunction-based CC2 benchmark calculations, they still yield serious errors in excitation energy trends. Based on an analysis of electron-hole transition density matrices, we also show that conventional hybrid functionals overdelocalize excitons and underestimate quasiparticle energy gaps in the acene systems. The results of the present study emphasize the importance of a range-separated and asymptotically-correct contribution of exchange in TDDFT for investigating optoelectronic and excitonic properties, even for these simple valence excitations.

Acknowledgement

This research was supported in part by the National Science Foundation through TeraGrid resources (Grant No. TG-CHE1000066N) provided by the National Center for Supercomputing Applications.

Contents

Introduction

Conjugated organic structures have attracted significant recent attention due to their potential applications in single-molecule transistors and organic photovoltaics. In the quest for smaller and more efficient electronics, organic semiconductors serve as a promising alternative to their silicon counterparts because of their increased electronic efficiency and ease of chemical functionalization.[1] In this context, oligoacenes which are composed of linearly fused benzene rings (Figure 1) have high application potential since they possess large charge-carrier mobilities and tunable electronic band gaps. Most notably, pentacene is already utilized as an organic field-effect transistor due to its large hole mobility (5.5 cm2/V·s) which exceeds that of amorphous silicon.[2,3] In general, the linear acenes are especially important since they form the basic fundamental units of zig-zag graphene nanoribbons which continue to garner enormous interest as novel nanoscale materials.

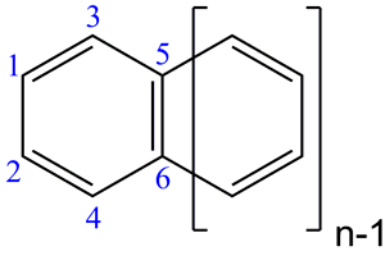

Figure 1. Molecular structure and atom labels for the linear acenes. The specific atom numbers depicted in this figure define an ordered basis for generating the transition density matrices in Figure 4.

Despite their promising photovoltaic applications, the oligoacenes are also noteworthy as a very unique system in which the successes and failures of time-dependent density functional theory (TDDFT) can be assessed and addressed. In 2003, Grimme and Parac noted a dramatic failure (0.5 eV error in excitation energies) of TDDFT using standard hybrid functionals for the low-lying $\pi \rightarrow \pi^*$ states of the oligoacenes.[4] Their findings were particularly unusual since these types of valence excitations are typically well described (within 0.1 eV) by hybrid TDDFT calculations. While it is well-known that long-range charge-transfer and Rydberg excitations provide a significant challenge for TDDFT,[5-9] these effects are not present in the acene systems since none of the valence excitations possess Rydberg character or involve any long-range charge transfer (the ground- and excited-state dipole moments are both zero by molecular symmetry). As a result, the unexpected failure of TDDFT in these very simple valence excitations is most unusual and somewhat unsettling.

The present study has two aims. First, we show that range-separated functionals,[10-12] which incorporate a position-dependent admixture of Hartree Fock exchange, yield substantial improvements over conventional hybrids for these various oligoacene excitations. Numerical optimization of parameters in both the range-separated and hybrid functionals are carried out to understand their effect on the excitation energies. Following the two-dimensional real-space

analysis approach of Tretiak et al.,[13-16] we then examine excitonic effects for the various excitations and TDDFT methods. The transition densities and electron difference density maps enable us to understand why conventional hybrids fail and how range-separated functionals accurately reproduce excitation energies and quasiparticle energy gaps for each of the different transitions. We begin by briefly reviewing these two different formalisms and then compare their accuracy in predicting oligoacene excitation properties.

Theory and Methodology

Recall that DFT is an exact theory in which the only inaccuracies encountered in practice arise from approximations to the exchange-correlation energy. In the conventional B3LYP hybrid functional,[17] the exchange-correlation energy has a relatively simple formulation given by

$$E_{xc} = a_0 E_{x,\mathrm{HF}} + \left(1 - a_0\right) E_{x,\mathrm{Slater}} + a_x \Delta E_{x,\mathrm{Becke88}} + \left(1 - a_c\right) E_{c,\mathrm{VWN}} + a_c \Delta E_{c,\mathrm{LYP}},$$

where $E_{x,\mathrm{HF}}$, $E_{x,\mathrm{Slater}}$, and $E_{x,\mathrm{Becke88}}$ are exchange contributions due to HF orbitals, Slater's uniform electron gas expression, and Becke's GGA model, respectively. The correlation contributions $E_{c,\mathrm{VWN}}$ and $E_{c,\mathrm{LYP}}$ arise from the corresponding Vosko-Wilk-Nusair and Lee-Yang-Parr correlation functionals. In this "global hybrid," the fraction of nonlocal HF exchange is held constant in space and has a specific value of $a_0 = 0.20$ for the B3LYP functional. In contrast to conventional hybrid functionals, the LC formalism[11,12] mixes HF exchange densities based on interelectronic distances by partitioning the electron repulsion operator $1/r_{12}$ into short-and long-range components as

$$\frac{1}{r_{12}} = \frac{1 - \mathrm{erf}\left(\mu r_{12}\right)}{r_{12}} + \frac{\mathrm{erf}\left(\mu r_{12}\right)}{r_{12}}.$$

The "erf" term denotes the standard error function, $r_{12} = |r_1 - r_2|$ is the interelectronic distance between electrons at coordinates r_1 and r_2, and μ is the range-separation parameter having units of Bohr^{-1}. The first term in the above equation is a short-range interaction which decays rapidly on a length scale of $\sim 2/\mu$, and the second term is the long-range part of the Coulomb potential. For a pure density functional (i.e. BLYP or PBE) which does not already include a fraction of nonlocal HF exchange, the exchange-correlation energy according to the LC formalism is

$$E_{xc} = E_{c,\mathrm{DFT}} + E_{x,\mathrm{DFT}}^{\mathrm{SR}} + E_{x,\mathrm{HF}}^{\mathrm{LR}},$$

where $E_{c,\mathrm{DFT}}$ is the correlation contribution, $E_{x,\mathrm{DFT}}^{\mathrm{SR}}$ is the short-range exchange functional and $E_{x,\mathrm{HF}}^{\mathrm{LR}}$ is the HF contribution to exchange computed with long-range part of the Coulomb operator.

For the linear acenes in this work, we investigated the performance of a long-range-corrected LC-BLYP functional against B3LYP and wavefunction-based CC2 calculations. To understand the role of different HF exchange schemes in the LC and conventional hybrids, we also explored the effect of optimizing the range parameter μ in LC-BLYP and the result of varying the global HF exchange fraction, a_0, in the B3LYP functional. In order to maintain a consistent comparison across the LC-BLYP, B3LYP, and CC2 levels of theory, identical molecular geometries and cc-PVTZ basis sets were used for each of the methods. These reference geometries were optimized at the B3LYP/cc-PVTZ level of theory.

We focus on two different valence excitations in the linear acenes, labeled in the literature[4,18] as L_a (lowest excited state of B_{2u} symmetry) and L_b (B_{3u} symmetry). As benchmarks for comparison, we calculated CC2/cc-PVTZ excitation energies of the linear acenes ranging from n = 2 to 7 benzene rings at the same reference molecular geometries. We take the CC2 results as reliable reference values since they accurately reproduce experimental excitation energies[4] and are close to CC3 benchmark calculations in the smaller acenes.[19] To investigate the effect of modifying the global HF exchange contribution in the acenes, we computed L_a and L_b excitation energies as a function of a_0. Similarly, we also computed the same excitations as a function of μ in the long-range-corrected LC-BLYP functional (we found that other long-range-corrected functionals such as LC-PBE and LC-BOP gave similar results). Using the CC2 excitations as reference values, we performed a total root-mean-square error (RMSE) analysis for all 12 energies (6 L_a and 6 L_b transitions) as a function of μ and a_0. Based on these results, we find that the RMSE in LC-BLYP has a minimum at μ = 0.29 $Bohr^{-1}$ with a RMS error of 0.10 eV (perhaps, surprisingly, this RMSE-optimized value of μ is nearly identical to the 0.31 $Bohr^{-1}$ value recommended for simultaneously describing excitation and fluorescence energies in oligothiophenes[20]). The RMSE in the B3LYP-like global hybrid functional has a minimum at a_0 = 0.50, with a larger error of 0.20 eV. We denote this re-optimized hybrid functional with a_0 = 0.50 as $B3LYP_{opt}$ in the remainder of this work. Unless otherwise noted, all further LC-BLYP calculations indicate a range-separation parameter of μ = 0.29 $Bohr^{-1}$.

Results and Discussion

Table 1 compares the L_a and L_b excited-state energies between B3LYP, $B3LYP_{opt}$, LC-BLYP and CC2, and Figures 2a and 2b depict in more detail the general trends in transition energies (expressed in wavelength units) between the various TDDFT and CC2 results. It is important to note in these figures that the energetic ordering of the two electronic states is different, depending on the size of the acene. Specifically, both CC2 and experimental studies indicate a curve crossing between the L_a and L_b states occurs slightly before n = 3 benzene rings (anthracene). For all of the other larger acenes, the L_a state lies energetically below the L_b state. Examining Table 1 and Figure 2b, we find that the LC-BLYP calculations are unique in that they show excellent agreement with CC2 energies for both the L_a and L_b excitations. Moreover, the LC-BLYP method preserves the correct ordering of electronic states between n = 2 and n = 3 benzene rings. In contrast, Figure 2a shows that the B3LYP global hybrid severely

underestimates excitation energies (i.e. overestimates absorption wavelengths) for the L_a electronic state. The situation is somewhat improved upon using the RMSE-optimized $a_0 = 0.50$ value in B3LYP$_{opt}$; however, this procedure results in L_b excitations which are now overestimated and L_a excitations which are still quite underestimated. Most importantly, both B3LYP and B3LYP$_{opt}$ give an incorrect ordering of electronic states – the crossing between L_a and L_b curves occurs much too early in both functionals, and the electronic symmetries in naphthalene have the wrong order. In general, the accuracy in excitation energies and trends is significantly improved with the LC scheme, while conventional hybrids are unable to reproduce the qualitative behavior in excitations even if the fraction of HF exchange is optimized.

Number of rings	B3LYP ($a_0 = 0.20$)	B3LYP$_{opt}$ ($a_0 = 0.50$)	LC-BLYP ($\mu = 0.29$)	CC2
		L_a State		
2	4.39 (283)	4.69 (265)	4.76 (261)	4.89 (254)
3	3.22 (386)	3.54 (350)	3.63 (341)	3.70 (335)
4	2.44 (509)	2.75 (451)	2.88 (431)	2.90 (427)
5	1.89 (656)	2.19 (567)	2.35 (528)	2.35 (528)
6	1.49 (834)	1.77 (699)	1.96 (631)	1.95 (635)
7	1.18 (1050)	1.46 (849)	1.68 (740)	1.66 (748)
		L_b State		
2	4.48 (277)	4.75 (261)	4.59 (270)	4.47 (277)
3	3.87 (320)	4.14 (300)	4.02 (309)	3.90 (318)
4	3.48 (357)	3.73 (332)	3.65 (340)	3.52 (352)
5	3.21 (386)	3.46 (359)	3.39 (365)	3.27 (379)
6	3.02 (411)	3.26 (381)	3.22 (386)	3.09 (401)
7	2.88 (431)	3.11 (399)	3.08 (402)	2.97 (418)

Table 1. Comparison of TDDFT and CC2 excitation energies [eV] (wavelengths [nm] are in parentheses) for L_a and L_b states in linear acenes. The B3LYP$_{opt}$ functional denotes a modified B3LYP functional with a RMSE-optimized exchange fraction of $a_0 = 0.50$, as discussed in the main text. Excitation energies were computed with the cc-pVTZ basis with the same reference geometry for all of the different methods.

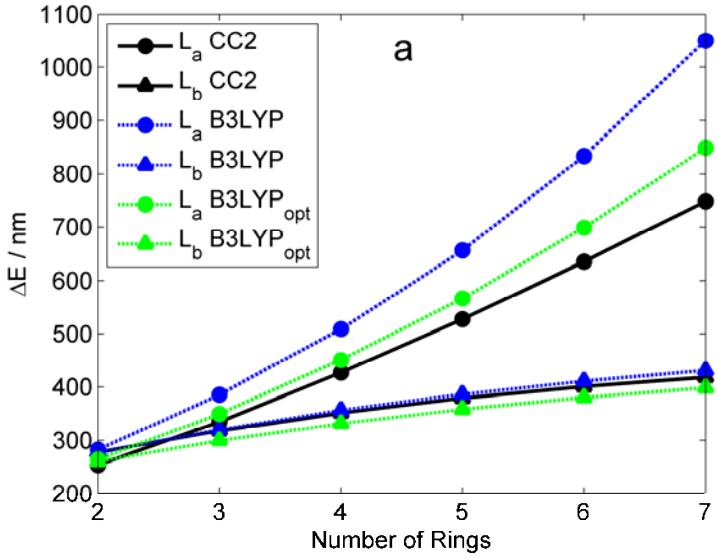

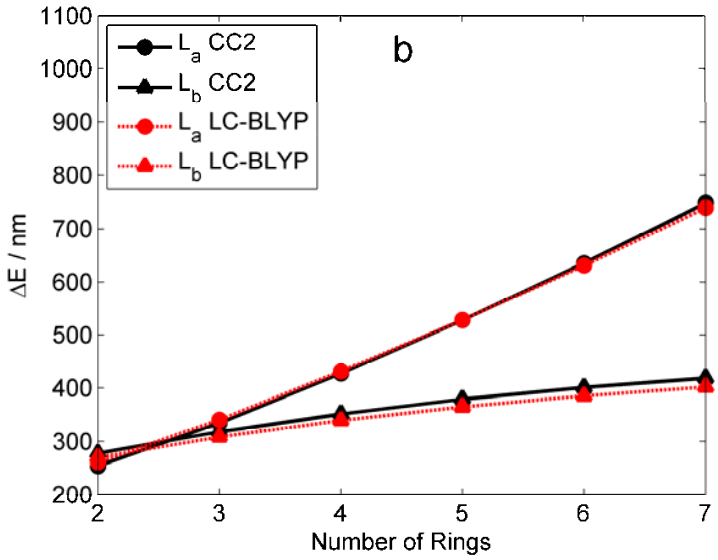

Figure 2. Comparison between TDDFT and CC2 excitation energies (in wavelength units) for (a) conventional global hybrid and (b) range-separated LC-BLYP functionals. The B3LYP$_{opt}$ functional denotes a modified B3LYP functional with a RMSE-optimized exchange fraction of a_0 = 0.50, as discussed in the main text.

From these results, it is interesting to note that long-range charge transfer is not responsible for the unexpected failure of B3LYP in these highly-symmetrical systems. In a recent theoretical study, Peach et al.6 introduced a diagnostic test which essentially measures the spatial overlap, Λ, between the occupied and virtual orbitals involved in an excitation. Based on their extensive benchmarks, if Λ is less than 0.3, indicating little overlap and significant long-range charge transfer character, hybrid functionals are predicted to yield inaccurate results. We computed the Λ diagnostic for both the L_a and L_b states in the acenes and found that all values were well above the 0.3 threshold (some of them even approaching 0.9), indicating a substantial overlap and no long-range charge transfer in these systems. Thus, instead of long-range charge transfer from one

end of the molecule to the other, we find that the L_a excitation involves a sizeable local rearrangement of electron density. In support of this assertion, Figure 3 depicts the electron density difference map ($\rho_{\text{excited}} - \rho_{\text{ground}}$) for the L_a and L_b excited states in pentacene computed at the CC2 level of theory. The electron density difference map gives a dynamic visualization of electronic rearrangement for a transition, with red regions (positively valued) denoting an accumulation of density and blue regions (negatively valued) representing a depletion of density upon excitation. As depicted in Figure 3, the L_a state involves significantly more local charge redistribution than the higher-energy L_b state. In particular, the L_b excited-state density is very similar to the ground state, as evidenced by the very small and sparsely-distributed isosurface regions. Notice also that the length scale of charge redistribution is on the order of the carbon-carbon bond length (~1.4 Å), which is comparable to the length scale at which LC-BLYP predicts long-range HF exchange to dominate short-range DFT correlation ($1/\mu$ ~ 1.8 Å). Even though none of these transitions have long-range charge transfer character, our findings support the physical interpretation that a range-separated contribution of full HF exchange on the length scale of the molecule is still necessary for accurately describing these local charge rearrangements.

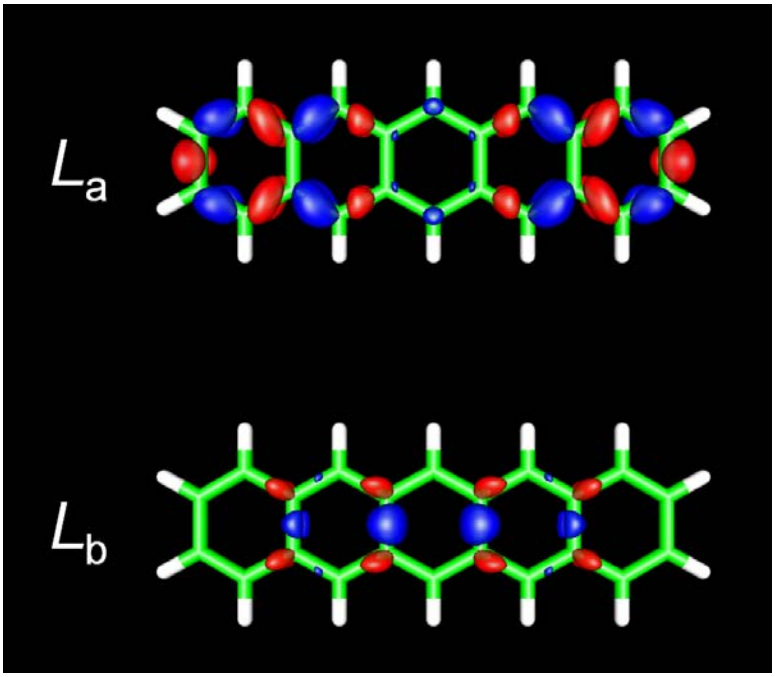

Figure 3. Electron density difference maps ($\rho_{\text{excited}} - \rho_{\text{ground}}$) for the L_a and L_b excited states of anthracene computed at the CC2 level of theory. Red regions denote a positive density difference (accumulation of density upon electronic excitation), and blue regions represent a negative density difference (depletion of density upon excitation). Both densities are plotted using the same isosurface contour value.

In order to provide further insight into these optoelectronic trends, we carried out an investigation of excitonic effects by analyzing electron-hole transition density matrices for the various excitations and TDDFT methods. In figure 4, we plot the absolute value of the coordinate density matrix elements, $\left|\left(Q_v\right)_{mn}\right| = \left|\left\langle \psi_v \left| c_m^\dagger c_n \right| \psi_g \right\rangle + \left\langle \psi_g \left| c_m^\dagger c_n \right| \psi_v \right\rangle\right|$, for the L_a and L_b

excitation energies computed at the LC-BLYP level of theory. In this compact expression, ψ_g and ψ_v are ground and excited states, respectively, and the Fermi operators $c_i^\dagger$ and c_i represent the creation and annihilation of an electron in the *i*th basis set orbital in ψ. As described in previous work,[12-15] the $\mathbf{Q_v}$ matrix forms a two-dimensional *xy* grid running over all the carbon sites along the *x* and *y* axes. The specific ordering of the carbon sites used in this work is shown in Figure 1. In short, the $(Q_v)_{mn}$ matrix provides a panoramic view of exciton delocalization by representing the joint probability amplitude of an electron being at position *m*, and a hole at site *n*. Based on this construction, off-diagonal elements with large intensities represent widely-separated electron-hole pairs between different atoms. As shown in Figure 4, the L_a density matrix has more off-diagonal elements than the corresponding L_b excitation, whose matrix elements are primarily confined along the diagonal. These figures reflect the more delocalized nature of the L_a state, in agreement with the electron density difference maps discussed previously. It is also important to note that all the transition density plots are symmetric along the counterdiagonal, verifying that no long-range charge transfer occurs in these systems (an asymmetric transition density along the counterdiagonal implies more electrons than holes are localized on one side of the molecule).

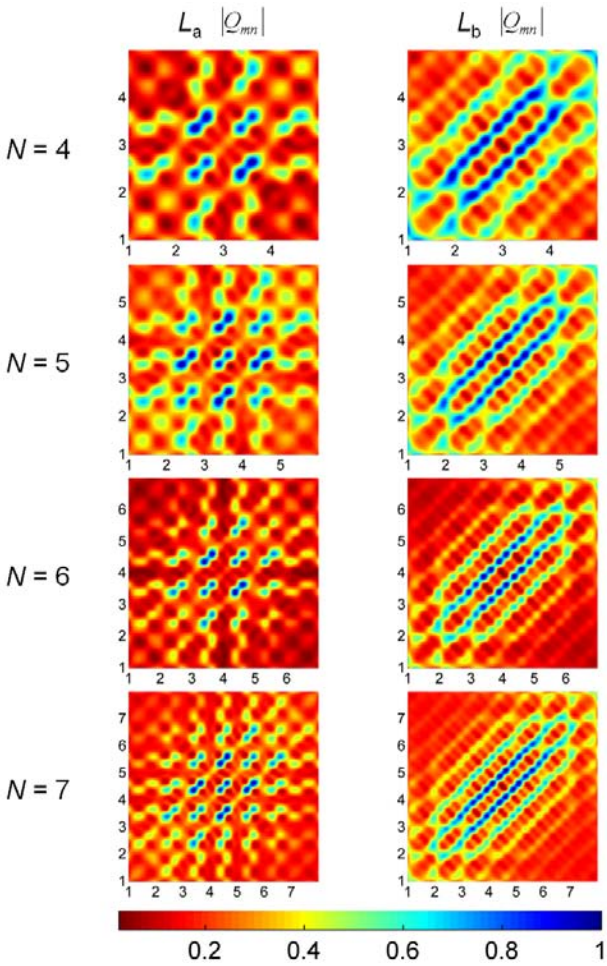

Figure 4. Contour plots of coordinate density matrices (**Q**) for the L_a and L_b excited states computed at the LC-BLYP level of theory. The *x*- and *y*-axis labels represent the number of benzene repeat units in the molecule. The elements of the coordinate matrix, Q_{mn}, give a measure of exciton delocalization between sites m (*x* axis) and n (*y* axis). The color scale is given at the bottom.

Finally, to compare excitonic effects in global and range-separated hybrids, we also computed transition density plots for both the B3LYP and LC-BLYP functionals. For both the L_a and L_b states, the B3LYP functional gives a more delocalized density-matrix pattern compared to the LC-BLYP functional. These findings are consistent with the B3LYP formalism which incorporates a global fraction of 20% HF exchange and, therefore, exhibits a -0.2/*r* dependence for the exchange potential. As a result, the asymptotically-incorrect B3LYP exchange potential is not attractive enough, simultaneously leading to an over-delocalized electron-hole pair and a severely underestimated quasiparticle energy gap (the quasiparticle gap can be approximated by the difference between the lowest unoccupied and highest unoccupied molecular orbital energies, $E_{LUMO} - E_{HOMO}$). Closely related to this underestimation of quasiparticle energies, it is interesting to note that the B3LYP functional gives inconsistent electronic properties as required by an exact functional. In exact Kohn-Sham theory, the energy of the highest occupied molecular orbital is equal to the negative of the ionization energy. For the pentacene molecule as a specific example, the B3LYP functional provides a $-E_{HOMO}$ value of 4.78 eV which significantly underestimates the experimental ionization energy21 of 6.61 eV. In contrast, the LC formalism, which incorporates a correct asymptotic behavior of the exchange potential by construction, gives a $-E_{HOMO}$ value of 6.69 eV, in exceptional agreement with experiment (the excellent agreement between the $-E_{HOMO}$ values in LC-BLYP and the experimental ionization energies also holds for the other acenes).

Conclusion

In conclusion, the present study clearly indicates that a range-separated contribution of exchange plays a vital role in predicting optoelectronic properties in the linear acenes. Even though none of the excitations involve long-range charge transfer, we find that a range-separated contribution of full HF is still necessary to accurately describe the local valence excitations in these systems. Re-optimizing the fraction of exchange in a global hybrid like B3LYP moderately improves the description of the L_a excited state; however, this same procedure also corrupts the balance between exchange and correlation errors with the L_b excited states becoming severely overestimated. In particular, global hybrid functionals overdelocalize excitons, underestimate quasiparticle energies, and are unable to reproduce general trends in both L_a and L_b, even if the fraction of HF exchange is optimized. As acenes form the basis of graphene sheets and nanoribbons, this study serves an important role in determining which TDDFT methods are most appropriate for these systems, especially since wavefunction-based calculations on large graphene nanoribbons are prohibitively demanding. With this in mind, we anticipate that the LC-TDDFT technique will play a significant role in understanding and accurately predicting the optoelectronic properties in these novel nanostructures.

References

(1) Sun, S.; Sariciftci, N. S. Organic Photovoltaics: Mechanisms, Materials, and Devices; CRC Press: Boca Raton, FL, 2005.

(2) Koch, N. Organic Electronic Devices and Their Functional Interfaces. *ChemPhysChem* **2007**, *8*, 1438-1455.

(3) Hasegawa, T.; Takeya, J. Organic Field-Effect Transistors Using Single Crystals. *Sci. Technol. Adv. Mater.* **2009**, *10*, 024314.

(4) Grimme, S.; Parac, M. Substantial Errors from Time-Dependent Density Functional Theory for the Calculation of Excited States of Large π Systems. *ChemPhysChem* **2003**, *3*, 292-295.

(5) Dreuw, A.; Head-Gordon, M. Failure of Time-Dependent Density Functional Theory for Long-Range Charge-Transfer Excited States: The Zincbacteriochlorin−Bacteriochlorin and Bacteriochlorophyll−Spheroidene Complexes. *J. Am. Chem. Soc.* **2004**, *126*, 4007-4016.

(6) Peach, M. J. G.; Benfield, P.; Helgaker, T.; Tozer, D. J. Excitation Energies in Density Functional Theory: An Evaluation and a Diagnostic Test. *J. Chem. Phys.* **2008**, *128*, 044118.

(7) Rohrdanz, M. A.; Herbert, J. M. Simultaneous Benchmarking of Ground- and Excited-State Properties with Long-Range-Corrected Density Functional Theory. *J. Chem. Phys.* **2008**, *129*, 034107.

(8) Wong, B. M.; Cordaro, J. G. Coumarin Dyes for Dye-Sensitized Solar Cells: A Long-Range-Corrected Density Functional Theory. *J. Chem. Phys.* **2008**, *129*, 214703.

(9) Kozak, C. R.; Kistler, K. A.; Lu, Z.; Matsika, S. Excited-State Energies and Electronic Couplings of DNA Base Dimers. *J. Phys. Chem. B* **2010**, *114*, 1674-1683.

(10) Gill, P. M. W.; Adamson, R. D.; Pople, J. A. Coulomb-Attenuated Exchange Energy Density Functionals. *Mol. Phys.* **1996**, *88*, 1005-1009.

(11) Iikura, H.; Tsuneda, T.; Yanai, T.; Hirao, K. A Long-Range Correction Scheme for Generalized-Gradient-Approximation Exchange Functionals. *J. Chem. Phys.* **2001**, *115*, 3540-3544.

(12) Tawada, Y.; Tsuneda, T.; Yanagisawa, S.; Yanai, T.; Hirao, K. A Long-Range-Corrected Time-Dependent Density Functional Theory. *J. Chem. Phys.* **2004**, *120*, 8425-8433.

(13) Tretiak, S.; Chernyak, V.; Mukamel, S. Collective Electronic Oscillators for Nonlinear Optical Response of Conjugated Molecules. *Chem. Phys. Lett.* **1996**, *259*, 55-61.

(14) Mukamel, S.; Tretiak, S.; Wagersreiter, T.; Chernyak, V. Electronic Coherence and Collective Optical Excitations of Conjugated Molecules. *Science* **1997**, *277*, 781-787.

(15) Tretiak, S.; Igumenshchev, K.; Chernyak, V. Exciton Sizes of Conducting Polymers Predicted by Time-Dependent Density Functional Theory. *Phys. Rev. B* **2005**, *71*, 033201.

(16) Wong, B. M. Optoelectronic Properties of Carbon Nanorings: Excitonic Effects from Time-Dependent Density Functional Theory. *J. Phys. Chem. C* **2009**, *113*, 21921-21927.

(17) Becke, A. D. Density-Functional Thermochemistry. III. The Role of Exact Exchange. *J. Chem. Phys.* **1993**, *98*, 5648-5652.

(18) Platt, J. R. Classification of Spectra of Cata-Condensed Hydrocarbons. *J. Chem. Phys.* **1949**, *17*, 484-495.

(19) Kadantsev, E. S.; Stott, M. J.; Rubio, A. Electronic Structure and Excitations in Oligoacenes from Ab Initio Calculations. *J. Chem. Phys.* **2006**, *124*, 134901.

(20) Wong, B. M.; Piacenza, M.; Della Sala, F. Absorption and Fluorescence Properties of Oligothiophene Biomarkers from Long-Range-Corrected Time-Dependent Density Functional Theory. *Phys. Chem. Chem. Phys.* **2009**, *11*, 4498-4508.

(21) NIST Chemistry WebBook, NIST Standard Reference Database Number 69, Released June 2005 (http://webbook.nist.gov/chemistry).

Distribution

1	MS 0359	Donna L. Chavez
1	MS 9403	Bryan M. Wong (8223)
2	MS 9018	Central Technical Files (8944)
2	MS 0899	Technical Library (9536)